Available online at www.sciencedirect.com
ScienceDirect
Trans. Nonferrous Met. Soc. China 26(2016) 2170−2178
Transactions of Nonferrous Metals Society of China
www.tnmsc.cn

Determination of processing power and optimum billet radius of modified backward extrusion by upper bound approach

S. H. HOSSEINI, K. ABRINIA

School of Mechanical Engineering, College of Engineering, University of Tehran, 16846-13114, Tehran, Iran

Received 8 August 2015; accepted 31 January 2016

Abstract: A recently developed backward extrusion method entitled "modified backward extrusion" was presented using an upper bound analysis. For this purpose deformation area was divided into four distinct zones and a kinematically admissible velocity field for each of them was suggested. Total dissipated power was calculated for the deformation zones and the extrusion power was computed. The correlations of important geometrical parameters with extrusion force and dissipated powers were shown. Finding the initial billet size, a challenging area in the modified backward extrusion method, was discussed and the optimum billet radius was obtained, considering the minimum relative extrusion pressure. Finite element analyses were conducted and the results were compared with the upper bound analysis. Finally, experiments were executed on commercially pure aluminium and a good agreement between upper bound and finite element analyses with experimental values was observed.
Key words: modified backward extrusion; upper bound method; finite element analysis; optimum billet radius

1 Introduction

Among various manufacturing processes, backward extrusion process is an applicable metal forming method which has been extensively used in the manufacturing of close ended products [1]. Even though this method has significant advantages such as optimum material usage, high dimensional accuracy, desirable mechanical property and the ability to produce near net shape products, unstable deformation zone in this method creates a non-uniform strain distribution along the extruded work piece [2]. Therefore, obtaining products with uniform mechanical properties using a conventional backward extrusion is a big challenge [3].

Novel backward extrusion is the new extrusion process, in which the newly redesigned die setup provides lower processing power and uniform strain distribution along the extruded products by restricting the deformation zone in a fixed region [4]. In this method deformable billet is embedded in a mandrel and the material can just flow between the mandrel and the die. However, novel backward extrusion has lower power and gives more strain uniformity along the extruded work piece in comparison with the conventional backward extrusion [4]. This method was modified by authors to achieve higher strain value and more strain uniformity [5]. Figure 1 depicts a simple representation of modified backward extrusion which shows the punch, mandrel, die and billet. As can be seen in Fig. 1, deformable billet flows in a particular region which is stable, thus the more uniform strain distribution is achievable in this method [5].

Although a few analytical methods have been developed for metal forming analyses, upper bound analysis and finite element method have attracted more attention by researchers [6−9]. Though FEM gives a more accurate results than upper bound analysis, it is very time-consuming. For this case, upper bound analysis is an appropriate method which presents a good estimation of processing power, material flow and strain distribution using a lesser computational time [10]. There are some relevant studies regarding the upper bound analysis of conventional backward extrusion which will be presented next. WIFI et al [11] surveyed material flow and stress distribution during the extrusion process by a combined FE and upper bound method, verified by some examples of backward extrusion process. BAE and YANG [12] investigated backward extrusion process of the round billet to elliptical shaped product by three-dimensional velocity field by using upper bound approach. Also, they presented an admissible velocity

Corresponding author: S. H. HOSSEINI; Tel/Fax: +98-2161114026; E-mail: hadi_hosseiny@ut.ac.ir
DOI: 10.1016/S1003-6326(16)64333-9

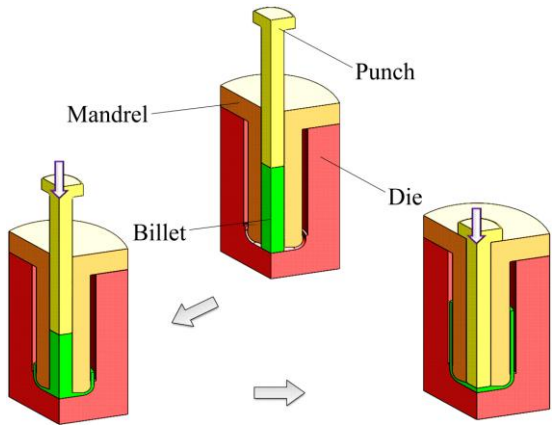

Fig. 1 Simple representation of modified backward extrusion tools

field for the backward extrusion of internally shaped tube from arbitrary shaped billet for calculating extrusion power [3]. MOSHKSAR and EBRAHIMI [13] studied backward extrusion of polygonal hollow components by implementing a spherical admissible velocity field. KIM and PARK [7] proposed an upper bound analysis of torsional backward extrusion, improving conventional backward extrusion difficulties, with low die rotation. ABRINIA and GHARIBI [6] surveyed backward extrusion of thin walled can by utilizing both of FE and upper bound analysis. As demonstrated, some analytical works were carried out on conventional backward extrusion, although there is no analytical study on recently developed modified backward extrusion. In addition, a fundamental issue with this method is introduction of a criterion regarding the determination of the optimum billet diameter. As a result, in this study an upper bound analysis of the modified backward extrusion process was presented, obtaining processing power and optimum billet diameter. Also, finite element analysis by DEFORM3D software was performed to make comparisons with the upper bound results. Finally, upper bound and FE results were verified by experimental data which were obtained from the tests on commercially pure aluminum.

2 Upper bound analysis

According to the upper bound theory, among the various admissible velocity fields, suggested for a deformable body, just one can have minimum energy consumption, corresponding to external input power. In other words, other admissible velocity fields which can satisfy compressibility condition overestimate the required processing power [14]. The total dissipated power of extrusion process J^* can be defined by the following equation:

$$J^* = \frac{2}{\sqrt{3}}\sigma_{\mathrm{av}}\int_V \sqrt{\frac{1}{2}\dot{\varepsilon}_{ij}\dot{\varepsilon}_{ij}}\,\mathrm{d}V + \frac{\sigma_{\mathrm{av}}}{\sqrt{3}}\int_{S_{\mathrm{v}}}|\Delta V|\mathrm{d}s + \frac{m\sigma_{\mathrm{av}}}{\sqrt{3}}\int_{S_{\mathrm{f}}}|\Delta V|\mathrm{d}s - \int_{S_{\mathrm{t}}} T_i V_i \mathrm{d}s \tag{1}$$

where σ_{av} is the mean flow stress, $\dot{\varepsilon}_{ij}$ is the strain rate tensor, ΔV is the velocity discontinuity on the friction and velocity discontinuity surfaces S_{f} and S_{v}, m is the friction factor, T_i is the traction force and V_i is the velocity imposed on the traction surface S_{t}. In fact, each part of Eq. (1) corresponds to a specific power, shown by

$$\begin{cases} \dot{W}_{\mathrm{i}} = \dfrac{2}{\sqrt{3}}\sigma_{\mathrm{av}}\displaystyle\int_V \sqrt{\frac{1}{2}\dot{\varepsilon}_{ij}\dot{\varepsilon}_{ij}}\,\mathrm{d}V \\ \dot{W}_{\mathrm{s}} = \dfrac{\sigma_{\mathrm{av}}}{\sqrt{3}}\displaystyle\int_{S_{\mathrm{v}}}|\Delta V|\mathrm{d}s \\ \dot{W}_{\mathrm{f}} = \dfrac{m\sigma_{\mathrm{av}}}{\sqrt{3}}\displaystyle\int_{S_{\mathrm{v}}}|\Delta V|\mathrm{d}s \\ \dot{W}_{\mathrm{t}} = \displaystyle\int_{S_{\mathrm{t}}} T_i V_i \mathrm{d}s \end{cases} \tag{2}$$

where $\dot{W}_{\mathrm{i}}$, $\dot{W}_{\mathrm{f}}$ and $\dot{W}_{\mathrm{s}}$ are the internal deformation power, the die-material friction power and the velocity discontinuity or shear power respectively, also $\dot{W}_{\mathrm{t}}$ is the traction force power. The strain rates in cylindrical coordinate are calculated by the following equations:

$$\begin{cases} \dot{\varepsilon}_{rr} = \dfrac{\partial V_r}{\partial r} \\ \dot{\varepsilon}_{\theta\theta} = \dfrac{1}{r}\dfrac{\partial V_\theta}{\partial \theta} + \dfrac{V_r}{r} \\ \dot{\varepsilon}_{zz} = \dfrac{\partial V_z}{\partial z} \\ \dot{\varepsilon}_{r\theta} = \dfrac{1}{2}\left(\dfrac{\partial V_\theta}{\partial r} + \dfrac{1}{r}\dfrac{\partial V_r}{\partial \theta} - \dfrac{V_\theta}{r}\right) \\ \dot{\varepsilon}_{rz} = \dfrac{1}{2}\left(\dfrac{\partial V_z}{\partial r} + \dfrac{1}{r}\dfrac{\partial V_r}{\partial z}\right) \\ \dot{\varepsilon}_{\theta z} = \dfrac{1}{2}\left(\dfrac{\partial V_\theta}{\partial z} + \dfrac{1}{r}\dfrac{\partial V_z}{\partial \theta}\right) \end{cases} \tag{3}$$

where V_r, V_θ and V_z are the velocities in directions of r, θ and z, respectively. Because of the axis of symmetry of modified backward extrusion process, the strain rates are simplified as follows:

$$\begin{cases} \dot{\varepsilon}_{rr} = \dfrac{\partial V_r}{\partial r} \\ \dot{\varepsilon}_{\theta\theta} = \dfrac{V_r}{r} \\ \dot{\varepsilon}_{zz} = \dfrac{\partial V_z}{\partial z} \\ \dot{\varepsilon}_{rz} = \dfrac{1}{2}\left(\dfrac{\partial V_z}{\partial r} + \dfrac{1}{r}\dfrac{\partial V_r}{\partial z}\right) \end{cases} \tag{4}$$

The fundamental principle in the metal forming analyses, incompressibility condition is given by

$$\dot{\varepsilon}_{rr}+\dot{\varepsilon}_{\theta\theta}+\dot{\varepsilon}_{zz}=0 \tag{5}$$

Substituting strain components into Eq. (5) gives

$$\frac{\partial V_r}{\partial r}+\frac{V_r}{r}+\frac{\partial V_z}{\partial z}=0 \tag{6}$$

Equation (6) indicates that velocity components are dependent, in other words, obtaining velocity in one direction can be arbitrary, therefore another is determined by incompressibility condition. Obviously, the determination of admissible velocity field for the deformation zone in the upper bound method is an important stage. Hence, according to the complexity of the particle's path through the deformation zone, this area is divided into four distinct areas which are depicted in Fig. 2. As can be seen in Fig. 2, in this analysis the geometrical parameters include initial billet radius R_0 and its height H, the radius of bottom of extruded product R_1, deformation zone thicknesses t_0 and t_1, the radii of the zone IV R_2 and R_3 and the mandrels slope α, respectively.

Dividing of the deformation zone leads to admissible velocity field for each zone, therefore the total power is obtained by calculating the dissipating powers, as mentioned above. As shown in Fig. 2 the cylindrical coordinate was performed in this analysis because of the axis of symmetry in the modified backward extrusion. In addition, considering deformation area in separated regions results in the fact that zone I just dissipates frictional power. But the other regions are affected by friction, velocity discontinuity and deformation power. Moreover, velocity discontinuity may occur on surfaces S_1 to S_4.

As mentioned before, only one of the velocity fields proposed for the deformable body consumes minimum energy. As a result, the linear function of the velocity field in the direction z not only overestimates dissipation power, but also leads to the calculation of other velocity components. Therefore, the velocity of the zone II in the direction z was proposed as follows:

$$V_{z2}=\frac{V_0 z}{t_0} \tag{7}$$

where V_0 is the velocity of movable punch. Substituting Eq. (7) into the incompressibility equation gives a differential equation. Solving this equation gives another component of the velocity field in the direction r which is defined by

$$V_{r2}=-\frac{V_0 r}{2t_0} \tag{8}$$

Continuing this procedure for zones III and IV leads to compute the velocity fields in these zones which are given by Eq. (9) and Eq. (10).

$$\begin{cases} V_{r3}=\dfrac{V_0 {R_0}^2}{2r(A+Br)} \\ V_{z3}=-\dfrac{V_0 {R_0}^2}{2}\left(\dfrac{Bz}{r(A+Br)^2}\right) \end{cases} \tag{9}$$

$$\begin{cases} V_{r4}=\dfrac{V_0 {R_0}^2}{2R_1R_2t_1}(R_3+z) \\ V_{z4}=\dfrac{V_0 {R_0}^2}{2R_1R_2}(r-R_1) \end{cases} \tag{10}$$

where V_{r3} and V_{z3} are the velocity components in the zone III respectively, $A=t_0+R_0\tan\alpha$, $B=-\tan\alpha$ and $\alpha=\tan^{-1}\left(\dfrac{t_0-t_1}{R_1-R_0}\right)$.

Substituting velocity components of each zone into strain rate tensor and calculating dissipated powers by integration in special boundaries lead to extrusion power $\dot{W}_{\text{tot}}$ and extrusion force F_{e} which are related by

$$F_{\text{e}}=\frac{\dot{W}_{\text{tot}}}{V_0} \tag{11}$$

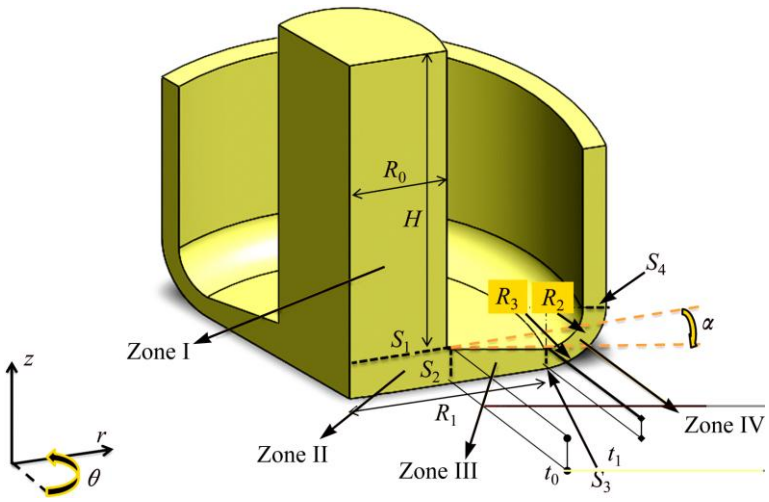

Fig. 2 Dividing deformation zone into four distinct regions and representation of geometrical parameters

3 Experimental and FE procedures

The experiments of modified backward were carried out on the commercially pure aluminum in this study (Fig. 3). The mechanical properties of the samples were extracted from the standard compression test by INSTRON 30-ton press according to ASTM: E9-04 at ambient temperature. The plastic behavior of the material was estimated by Holomon's equation $\sigma=K\varepsilon^n$ in which K and n are 111.4 MPa and 0.396, respectively. Initial as-cast aluminum billets were prepared by machining up to a diameter of 25 mm and height of 70 mm. Extrusion die was made of hot work steel H13 and then hardened up to HRC 55. The experiments were executed by a 200-ton Wykeham Farrance hydraulic press. Initial billets were extruded by ram speed of about 10 mm/min and special cup produced with 63 mm in outer diameter, 3 mm in wall thickness (t_1) and 5 mm in initial deformation zone thickness. Friction effect was reduced by using lubricant of graphite-grease combination [5].

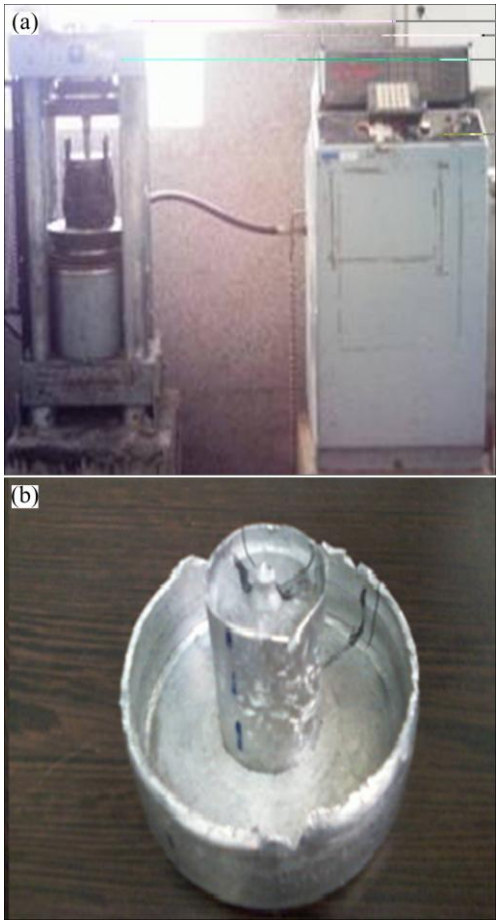

Fig. 3 Experimental setup of modified backward extrusion (a) and extruded product (b)

Finite element simulations were carried out by using DEFORM^{TM}3D software. Adaptive remeshing method, providing higher mesh quality, is specific characteristic of DEFORM software for the metal forming process with high amount of strains [15]. Initial billet and die component were modeled as deformable and rigid bodies in this simulation. The contact between the billet and the die was considered according to the constant shear model taking a friction factor between 0.1 to 0.4 [8,14]. The mesh sensitivity analysis was done by investigation of element number effect on the extrusion force. As can be seen on Fig. 4, increasing the element number reduces the extrusion force up to 6000 elements. Then extrusion force shows no considerable changes in the range of 6000−8000. FE analyses were simulated by total element number of 8000−10000 for a sector which was one-twelfth of the completed products. The element type used in these analyses was tetrahedral element with linear shape functions.

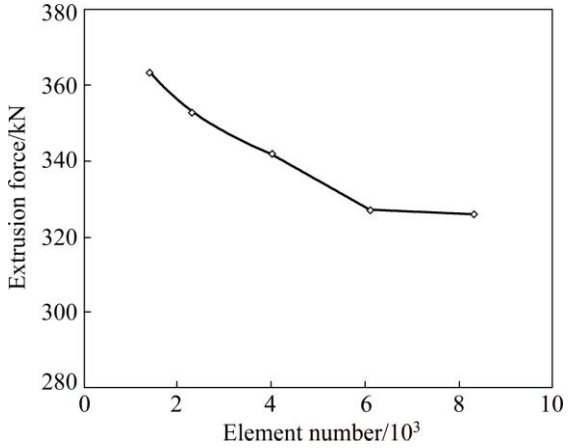

Fig. 4 Effect of element number on extrusion force

4 Results and discussion

4.1 Upper bound results

In this part upper bound results are presented by investigation of process parameters on extrusion force F_e, deformation power $\dot{W}_i$, velocity discontinuity power $\dot{W}_s$, friction power $\dot{W}_f$ and relative extrusion pressure P_e/σ_{av}. It is worth mentioning that for each figure some parameters were considered constant. Fixed parameters include: R_0=12.5 mm, R_1=50 mm, H=70 mm, t_1=3 mm, t_2=5 mm and R_2=10 mm. Figure 5 illustrates the effect of the initial billet radius on the extrusion force in different friction levels. As can be seen, increasing the initial billet radius and assuming that the other parameters were kept constant, extrusion force increases with a nonlinear trend. The reason is that the second deformation zone consumes more power, consequently extrusion force increases. Because of the nature of the process, the initial billet value must be chosen within specific limits. The lower limit can be determined by punch buckling probability and excessive punch displacement. And the upper level can be determined when required process

load for the modified backward extrusion corresponds to that of the conventional backward extrusion which is not satisfactory.

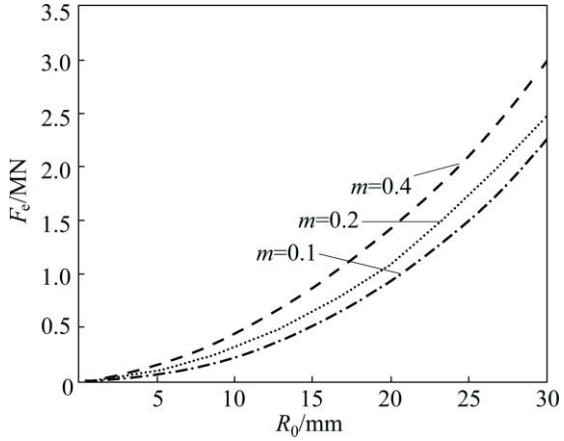

Fig. 5 Effect of initial billet radius on extrusion force in modified backward extrusion

Figure 6 depicts the effect of extruded part's radius on the extrusion force for different friction factors. As can be seen, the extrusion force has a linear correlation with the extruded part's radius. Increasing the R_0 rises the extrusion force, especially in higher friction values this is more significant. This trend can result from the excessive friction power, created by severe contact between the die and deformable body.

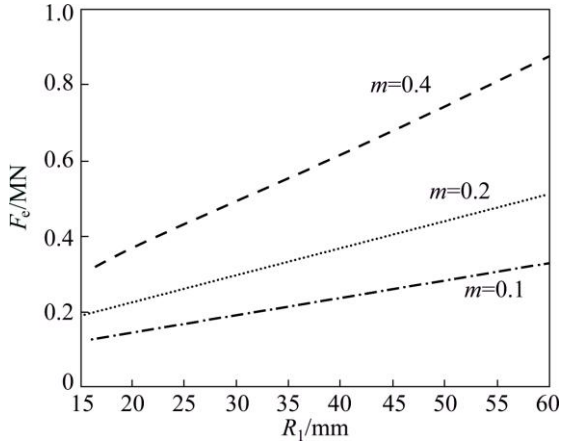

Fig. 6 Effect of extruded part's radius on extrusion force for different friction conditions

Other important geometrical parameters, such as extruded part's thickness, have a significant effect on extrusion force, which is illustrated in Fig. 7. As shown in Fig. 7, increasing the thickness decreases the extrusion force. It could be seen that for the lower thicknesses extrusion process much excessive power is needed, but after this limit the extrusion force does not change considerably and reaches a semi-stable condition. In other words, the extrusion force will be at this minimum level when the extruded part's thickness is in semi-stable condition. However, this parameter depends on the product's features and it is not under control.

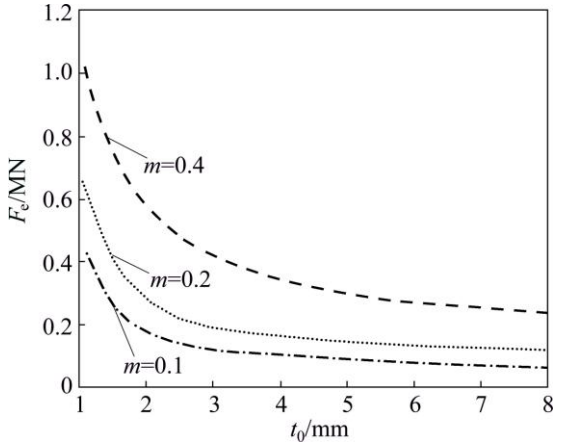

Fig. 7 Effect of extruded part's thickness on extrusion force in different friction condition

As mentioned above, the extrusion power includes deformation power $\dot{W}_i$, velocity discontinuity power $\dot{W}_s$, and friction power $\dot{W}_f$. Certainly, geometrical parameters play prominent roles in these powers. On the other hand, understanding the correlation between these parameters and the processing powers could be useful in various aspects. For example, when the main aim in the extrusion process is minimizing extrusion power and improving process efficiency, maximum internal power and minimum velocity discontinuity is needed [16,17], but when the texture refinement is a basic purpose especially in severe plastic deformation, the maximum velocity discontinuity can be beneficial in this process [18,19]. Figure 8 shows the effect of the initial billet radius on processing powers, by assuming that other parameters are constant, where $\dot{W}_{tot}$ is the total extrusion power. It can be seen that when the initial billet radius increases, the extrusion power is increased and also two separated limits are recognizable at a special

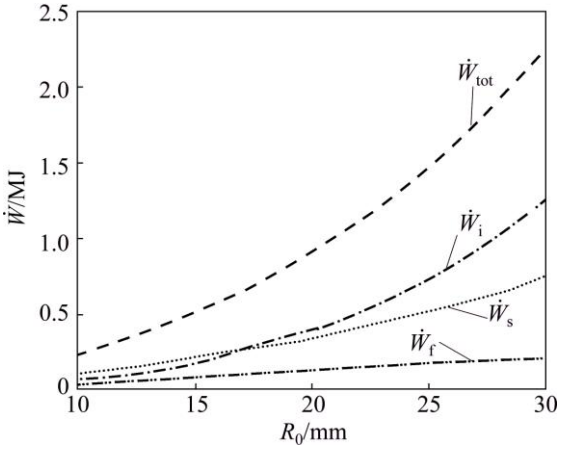

Fig. 8 Correlation between initial billet radius and processing power

value of billet radius of 19 mm. On the left side of this value $\dot{W}_s$ is dominant, but on the other side $\dot{W}_i$ is predominant and more efficiency can be obtained in this limit, but for bigger billet radii the extrusion force increases intensively.

Figure 9 illustrates the correlation of the extruded product's thickness with the extrusion power. As depicted, $\dot{W}_s$ and $\dot{W}_f$ values reduce with the increase in the thickness, but $\dot{W}_i$ remains nearly constant. The extrusion force reduces when the thickness increases. It could be inferred that increasing the extrusion force could not be attributed to deforming power $\dot{W}_i$. In addition, the process efficiency enhances when $\dot{W}_s$ and $\dot{W}_f$ decrease. In other words, increasing the process efficiency in thicker products could be attributed to the reduction of the velocity discontinuity and friction power values.

The effect of the extruded product's radius on processing powers is depicted in Fig. 10. It can be seen that $\dot{W}_f$ and $\dot{W}_i$ increase when R_1 enhances by a linear trend but $\dot{W}_s$ does not change. It can be concluded that the increase in R_1 has no effect on velocity discontinuity surfaces and therefore $\dot{W}_s$ remains unchanged.

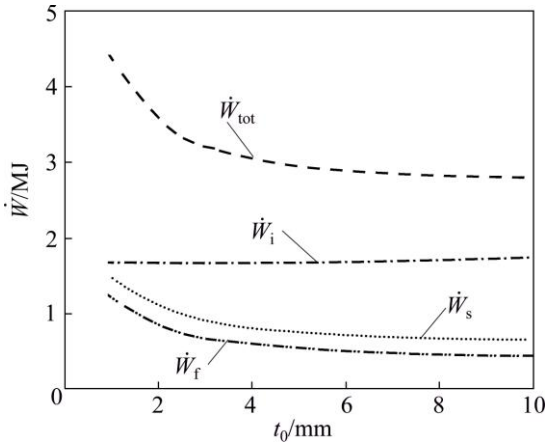

Fig. 9 Correlation of extruded product's thickness with processing powers

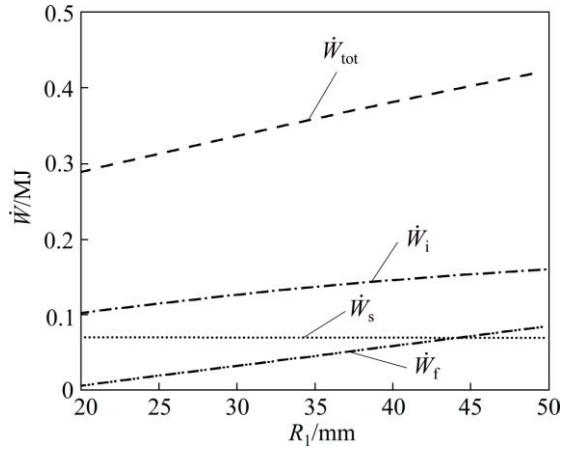

Fig. 10 Effect of extruded product's radius on processing power

As mentioned before, the relative extrusion pressure P_e/σ_{av} is an important output for upper bound analysis, but it correlates with geometrical parameters similar to that of the extrusion force except for the values of initial billet radii. Figure 11 illustrates the effect of initial billet radius on the relative extrusion pressure for different product's thicknesses. It can be seen that relative extrusion pressure has a bimodal trend, in which P_e/σ_{av} initially reduces to a certain value and then starts to increase. Unlike the other graphs of extrusion powers and force versus R_0, the minimum level of R_0 can be obtained from these curves. It can be obtained that the optimum billet radius, the big challenge of the modified backward extrusion, could be computed using the present analysis. Also, it could be concluded from Fig. 11 that the optimum radius increases for thicker products, which is satisfactory because when the thickness increases the punch displacement reduces, shorter punch is required and probable damage to the punch could be avoided.

The effect of friction factor on optimum billet diameter is shown in Fig. 12. It can be seen that the

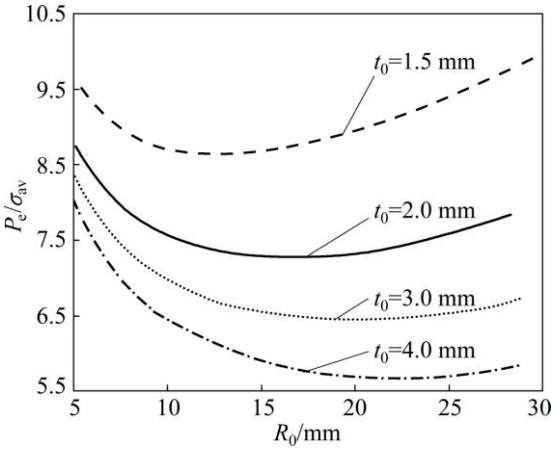

Fig. 11 P_e/σ_{av} vs R_0 graph of modified backward extrusion for different thicknesses

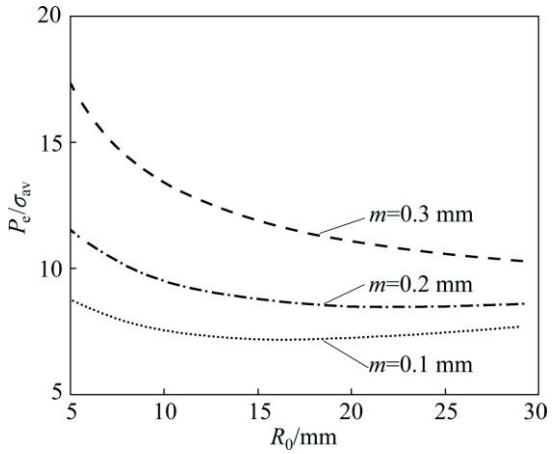

Fig. 12 P_e/σ_{av} vs R_0 graph of modified backward extrusion considering effect of friction

optimum billet diameter increases when friction factor goes up.

4.2 FEA and experiment

Figure 13 demonstrates the finite element analysis of a typical sample during modified backward extrusion in three steps. It can be seen that plastic deformation is concentrated in specific areas. This limits the plastic deformation and consequently reduces the extrusion force in comparison with the conventional backward extrusion [4]. The load−stroke diagram of FEM simulation for the modified backward extrusion, for different friction factors, is shown in Fig. 14, in which the three demonstrated steps of Fig. 13 are also illustrated by hollow stars.

When the extrusion process starts, initial billet flows into the deformation region and the extrusion force increases. Figure 13(a) is a representative of this period. When the deformation area is completed the extrusion load reaches a maximum level and the process transfers to stable condition (Fig. 13(b)). Finally, as shown in Fig. 14 the extrusion force reduces slightly. Decreasing the extrusion force after stable condition could be attributed to the reduction of the initial billet height and diminishing of the friction force.

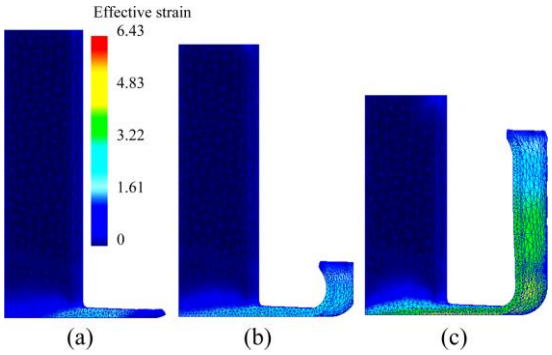

Fig. 13 Finite element analysis of modified backward extrusion

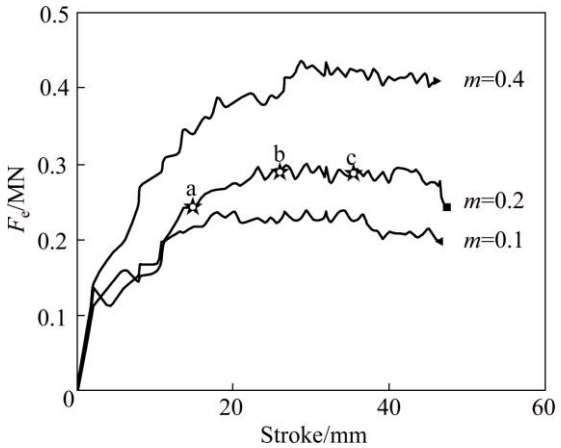

Fig. 14 Load−stroke diagram of FE procedure of modified backward extrusion

FEA and upper bound analysis (UBA) results with respect to the extrusion force, considering the effect of initial billet radius, are compared in Fig. 15. It is clear that by increasing the value of R_0, UBA results diverge from FE analyses. It may be attributed to the purposed velocity field for the second deformation zone, which could cause more discrepancy in the output data, although the same trend in both of FE and UB curves is observed.

Figure 16 demonstrates F_e−R_1 diagram for both of FE and UB analyses. UB results converge to FE when R_1 increases. In other words, when R_1 increases UB analysis shows more accuracy and gives better estimation. But when t_1 increases no considerable change occurs between FE and UB results as illustrated in Fig. 17. It means that the present velocity field accuracy is not influenced by thicker products.

The numerical results, including UBA and FEA, are compared with the experimental data as shown in Fig. 18. FEA and UBA were executed by a friction factor of 0.2 and experimental test dimensions. From Fig. 18 it could be seen that before the red dashed line FE data are higher than the experimental results. It may be attributed to

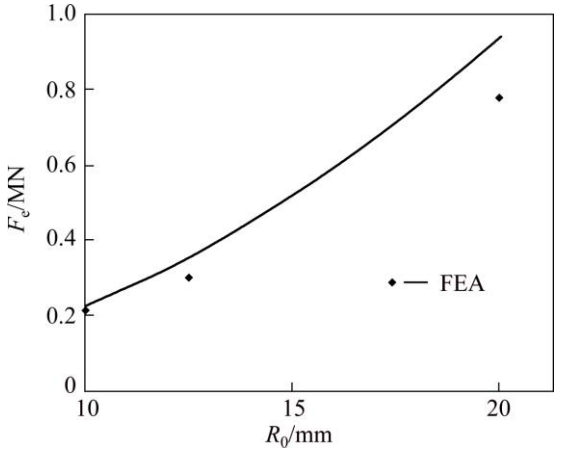

Fig. 15 Comparison of FEA and UBA results by consideration of initial billet radius effect

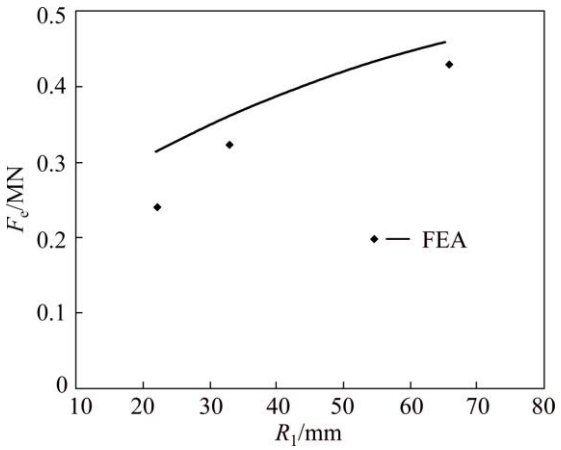

Fig. 16 F_e−R_1 diagram for both of FE and UB analyses

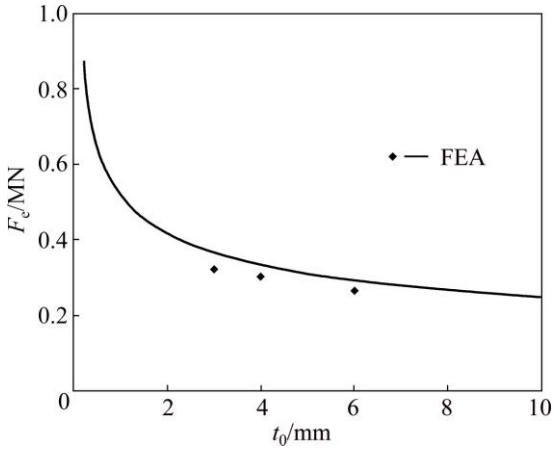

Fig. 17 Comparison of FEA and UBA results for various thicknesses

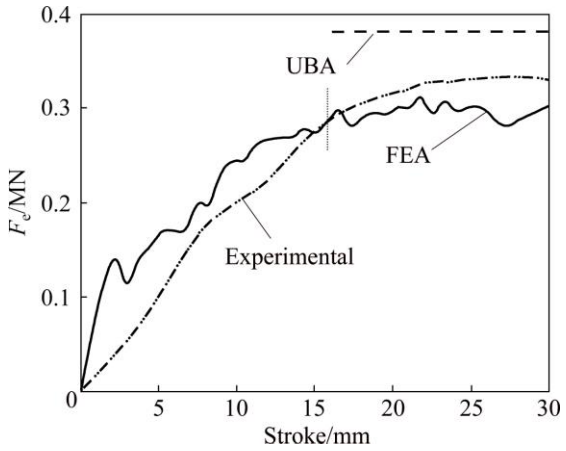

Fig. 18 Comparison of load−stroke curves resulted from FE, UB and experiment

suitable lubrication at the start of the process. But after a while lubricant escapes and friction forces increase and experimental curve overtakes FEA. Obviously, varying frictional conditions have not been considered in FE simulations, and constant friction condition was used. The pick extrusion forces resulting from FE, UB and experimental tests were 0.30, 0.33, and 0.37 MN respectively, showing a good agreement.

5 Conclusions

An upper bound analysis of recently developed backward extrusion method entitled “modified backward extrusion” was presented, and a kinematically admissible velocity field was determined for the modified backward extrusion. The proposed velocity field showed a good agreement with both of FEA and experimental results on commercially pure Al. The optimum billet radius was determined by minimizing the relative extrusion pressure versus initial billet radius, the correlations between processing powers and extrusion force with geometrical parameters were determined for the modified backward extrusion. Process efficiency was recognized by investigation of processing powers versus geometrical parameters, the convergence of the upper bound solution was examined by FE analyses.

References

[1] ABRINIA K, ORANGI S. Investigation of process parameters for the backward extrusion of arbitrary-shaped tubes from round billets using finite element analysis [J]. J Mater Eng Perform, 2009, 18: 1201−1208.

[2] FARHOUMAND A, EBRAHIMI R. Analysis of forward-backward-radial extrusion process [J]. Materials & Design, 2009, 30: 2152−2158.

[3] BAE W B, YANG D Y. An upper-bound analysis of the backward extrusion of tubes of complicated internal shapes from round billets [J]. Journal of Materials Processing Technology, 1993, 36: 157−173.

[4] SHATERMASHHADI V, MANAFI B, ABRINIA K, FARAJI G, SANEI M. Development of a novel method for the backward extrusion [J]. Materials & Design, 2014, 62: 361−366.

[5] HOSSEINI S H, ABRINIA K, FARAJI G. Applicability of a modified backward extrusion process on commercially pure aluminum [J]. Materials & Design, 2015, 65: 521−528.

[6] ABRINIA K, GHARIBI K. An investigation into the backward extrusion of thin walled cans [J]. Int J Mater Form, 2008, 1: 411−414.

[7] KIM Y H, PARK J H. Upper bound analysis of torsional backward extrusion process [J]. Journal of Materials Processing Technology, 2003, 143−144: 735−740.

[8] HAGHIGHAT H, MAHDAVI M M. Analysis and FEM simulation of extrusion process of bimetal tubes through rotating conical dies [J]. Transactions of Nonferrous Metals Society of China, 2013, 23: 3392−3399.

[9] HAGHIGHAT H, SHAYESTEH H. Upper bound analysis for hybrid sheet metals extrusion process through curved dies [J]. Transactions of Nonferrous Metals Society of China, 2014, 24: 3285−3292.

[10] KARAMI P, ABRINIA K. Development of a more realistic upper bound solution for the three-dimensional problems in the forward extrusion process [J]. Int J Mech Sci, 2013, 74: 112−119.

[11] WIFI A S, ABDULJABBAR Z S, SAKR M T. A combined UBET/FEM investigation of metal flow and stress analysis of dies in extrusion process [J]. Journal of Materials Processing Technology, 1990, 24: 431−440.

[12] BAE W B, YANG D Y. An upper-bound analysis of the backward extrusion of internally elliptic-shaped tubes from round billets [J]. Journal of Materials Processing Technology, 1992, 30: 13−30.

[13] MOSHKSAR M M, EBRAHIMI R. An analytical approach for backward-extrusion forging of regular polygonal hollow components [J]. Int J Mech Sci, 1998, 40: 1247−1263.

[14] HAGHIGHAT H, AMJADIAN P. A generalized velocity field for plane strain backward extrusion through punches of any shape [J]. Meccanica, 2013, 48: 2099−106.

[15] DEFORMTM 3D Version 6.1 (sp1) User’s Manual [M]. Vol. 1. Corporation SFT, 2007.

[16] LEE H, HWANG B, BAE W. A UBET analysis of non-axisymmetric forward and backward extrusion [J]. Journal of Materials Processing Technology, 2001, 113: 103−108.

[17] ABRINIA K, FARAHMAND P, PARCHAMI-SARGHIN M. Formulation of a new generalized kinematically admissible velocity field with a variable axial component for the forward extrusion of shaped sections [J]. Int J Adv Manuf Technol, 2013, 70: 1427−1435.

[18] FARAJI G, JAFARZADEH H, JEONG H J, MASHHADI M M, KIM H S. Numerical and experimental investigation of the deformation behavior during the accumulative back extrusion of an AZ91 magnesium alloy [J]. Materials & Design, 2012, 35: 251−258.

[19] FATEMI-VARZANEH S M, ZAREI-HANZAKI A, NADERI M, ROOSTAEI A A. Deformation homogeneity in accumulative back extrusion processing of AZ31 magnesium alloy [J]. Journal of Alloys and Compounds, 2010, 507: 207−214.

采用上限方法确定反挤压加工功和最优坯料半径

S. H. HOSSEINI, K. ABRINIA

School of Mechanical Engineering, College of Engineering, University of Tehran, 16846-13114, Tehran, Iran

摘　要：采用上限方法开发了一种新的改进反挤压方法。在这个方法中，将变形区划分为 4 个不同的区域，然后对每个区的运动许可速度场进行了设定。对变形区的总耗散功和挤压功进行了计算。对一些重要的几何参数与挤压力和耗散功的关系进行了探讨。考虑到最小的相对挤压压力，通过上限方法获得了最优的坯料半径。同时，采用有限元法对问题进行了分析并与采用上限方法获得的结果进行了比较。最后，将上限方法和有限元方法的计算结果与工业纯铝的实验结果进行了比较，结果表明他们之间吻合较好。

关键词：改进反挤压；上限方法；有限元分析；最优坯料半径

(Edited by Sai-qian YUAN)